Journal of Materials Chemistry C

Materials for optical and electronic devices

www.rsc.org/MaterialsC

Volume 1 | Number 12 | 28 March 2013 | Pages 2259–2380

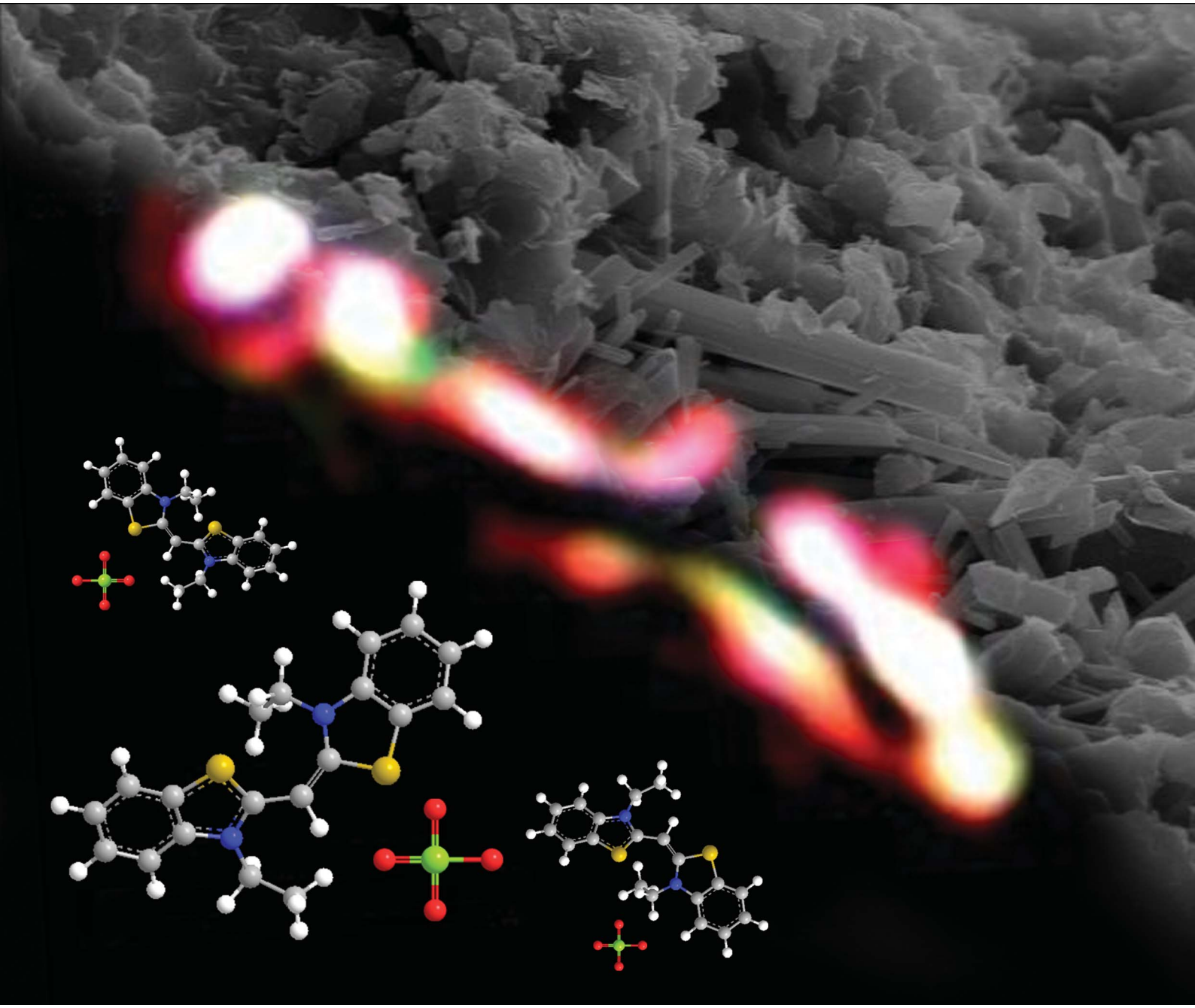

ISSN 2050-7526

RSC Publishing

PAPER

R. A. S. Ferreira, V. de Zea Bermudez *et al.*

Lamellar mono-amidosil hybrids incorporating monomethinecyanine dyes

2050-7526(2013)1:12;1-K

Journal of Materials Chemistry C

RSC Publishing

PAPER

View Article Online
View Journal | View Issue

Cite this: J. Mater. Chem. C, 2013, 1, 2290

Lamellar mono-amidosil hybrids incorporating monomethinecyanine dyes†

S. C. Nunes,[abc] C. B. Ferreira,[ab] J. Hümmer,[a] R. A. S. Ferreira,*[d] L. D. Carlos,[d] P. Almeida[ce] and V. de Zea Bermudez*[ab]

Received 29th October 2012
Accepted 13th January 2013

DOI: 10.1039/c3tc00515a

www.rsc.org/MaterialsC

Mono-amide cross-linked alkyl–siloxane hybrids synthesized through the sol–gel process and the self-directed assembly have been doped with variable concentrations of monomethinecyanines $SSCH_2(C_6H_5)I$, $SSCH_3Cl$ and $SSC_2H_5ClO_4$. The host matrix m-A(14) is a lamellar structured hybrid composed of short methyl-capped alkyl chains grafted to the siliceous framework through amide groups. The doped mono-amidosil hybrid materials were obtained as solid powders. The bulky $SSCH_2(C_6H_5)I$ dye inhibited the condensation of the silica network. In the $SSCH_3Cl$- and $SSC_2H_5ClO_4$-doped m-A(14)-based materials the original lamellar structure coexists with a new lamellar ordered phase with a lower interlamellar distance in which the alkyl chains adopt essentially all-*trans* conformations. The efficient encapsulation of these two dyes by m-A(14), which ensures their complete dissolution, is due to the coordination of the S atoms of $SSCH_3Cl$ and $SSC_2H_5ClO_4$ to the carbonyl oxygen atoms of the amide cross-links. This process leads to a major breakdown of the disordered and ordered hydrogen-bonded aggregates of m-A(14), but does not affect globally the strength of the hydrogen-bonded array. The most dilute $SSC_2H_5ClO_4$-doped mono-amidosil studied displays room temperature emission in the visible spectral region (380–680 nm) due to the convolution of the intrinsic emission (blue spectral region) of m-A(14) with that of the $SSC_2H_5ClO_4$ dye (green and red spectral regions) due to the formation of fluorescent J-dimers. The excitation spectra (monitored along the emission spectra) reveal the occurrence of host-to-monomethinecyanine energy transfer.

Introduction

Organic–inorganic hybrid materials[1,2] have attracted significant interest in materials science research,[3–5] primarily because their mechanical, physical and chemical properties can be designed and adjusted by changing the composition, the nature of the interactions established between the organic and inorganic components and the experimental conditions (*e.g.*, temperature, pH, solvent, catalyst). Additionally, organic–inorganic hybrid materials offer the advantages of both components, *i.e.*, the plasticity of the organic component and the thermal and dimensional stability of the inorganic counterpart.

Sol–gel chemistry[6] is one of the preferred methods for the preparation of advanced multifunctional organic–inorganic hybrid systems. The mild chemical conditions of this process allow the addition of dopants, such as organic dyes, to the host framework, yielding active materials with promising technological applications[7,8] in optics and photonics,[9–18] diagnostic and imaging,[19–21] dye-sensitized solar cells,[22] transparent colored coatings[23] and forensic investigation.[24]

Organic dyes intercalated within organic–inorganic host cages are known to exhibit significantly different properties from their solutions.[25] The incorporation of organic compounds into glasses prepared *via* the sol–gel method was first described in 1984 by Avnir *et al.*[26] who demonstrated the possibility of using the resulting materials as solid-state dye lasers. The intense research that followed this work involved the exploration of different types of dyes (*e.g.*, rhodamines,[13–16,27–33] cyanines[17,18,20,34] and perylimides[35]) and a variety of host matrices (*e.g.*, organically modified silicates (ormosils),[17,18,27,28,35] silica gels,[27,36] mesoporous silica,[29,31] silica nanoparticles[20] and composite glass–polymer frameworks[5,13,27,32,37,38]).

The main advantage of organic–inorganic hybrid cages for the encapsulation of dyes lies on their ability of, not only providing an adequate local environment for the dye in order to retain the strong fluorescent quantum yield, but also improving

[a]Chemistry Department, University of Trás-os-Montes e Alto Douro, Vila Real, Portugal. E-mail: vbermude@utad.pt; Fax: +351 259 350 480; Tel: +351 275 259 350 253
[b]CQ-VR, University of Trás-os-Montes e Alto Douro, 5001-801 Vila Real, Portugal. E-mail: vbermude@utad.pt; Fax: +351 259 350 480; Tel: +351 275 259 350 253
[c]Chemistry Department, Faculty of Sciences, University of Beira Interior, Covilhã, Portugal. E-mail: pjsa@ubi.pt; Fax: +351 275 319 730; Tel: +351 275 329 174
[d]Physics Department and CICECO, University of Aveiro, Aveiro, Portugal. E-mail: rferreira@ua.pt; Fax: +351 234 378 197; Tel: +351 234 378 103
[e]CICS-UBI – Centro de Investigação em Ciências da Saúde, University of Beira Interior, Covilhã, Portugal. E-mail: pjsa@ubi.pt; Fax: +351 275 319 730; Tel: +351 275 329 174

† Electronic supplementary information (ESI) available. See DOI: 10.1039/c3tc00515a

the dye's photostability. The tendency for the formation of organic aggregates is probably the major drawback of dye-doped organic–inorganic hybrids. The extent of the aggregation depends on the host–guest interaction. The formation of dimers can be deduced from the absorption and emission properties of the system: (a) non-fluorescent H dimers are characterized by a blue shifted absorption band (called H-band) with respect to the monomer absorption band and (b) fluorescent J dimers are characterized by a red shifted emission band (known as J-band) with respect to the monomer emission band.[39] Photoluminescence studies allow monitoring the presence of different aggregates in dye-containing hybrid systems and assessing the luminescent properties for specific applications. For example, the presence of J aggregates of polymethine dyes was investigated to produce laser active media.[39]

In the present work we have incorporated three cyanine dyes into a hierarchically structured ordered hybrid material named mono-amidosil (m-A(14))[40] with the goal of producing organized materials. We note that reports of dye-doped organic–inorganic hybrids with mesoscale periodicity and macroscale organization are scarce in the literature.[41–44] The studies conducted to date regard essentially dye-functionalized ordered mesoporous silica materials.[41–44]

Cyanine dyes,[45–49] the oldest known class of synthetic dyes, absorb from the ultraviolet (UV) to the infrared (IR) regions. These compounds are cationic polymethine dyes, which are planar, conjugated, open-chain (sometimes ring) systems of sp^2-hybridized carbon atoms with an odd number of methine groups and an even number of π electrons (Scheme 1).[45–49] The number of methine groups that join the two heterocyclic units determine the wavelength range of absorption of the dye, while the nature of the heterocyclic end ring has a smaller, but still significant effect on the wavelength range of the dye.[45–49] The chain length of the cyanine dye molecule is one of the most important structural factors dictating the optical features, since the increase by one –CH=CH– group results in a red shift of about 100 nm.[45–49] In general the longer wavelength cyanine dyes are less photostable than their shorter wavelength analogues.[50] The dye compounds used in the present investigation have been monomethinecyanines ($m = 0$), abbreviated by the notation ***SSRZ*** where X = Y = ***S***, ***R*** = CH_3, C_2H_5, $CH_2(C_6H_5)$ and ***Z*** = Cl, ClO_4 and I (Scheme 2).

The hybrid host matrix chosen, m-A(14), was obtained through the sol–gel process and self-assembly routes, and consists of 2D siliceous domains, separated by perpendicularly oriented alkyl chains, self-assembled through tail-to-tail van der Waals packing and intermolecular hydrogen bonds. Interestingly, in m-A(14) the reversible order–disorder phase transition

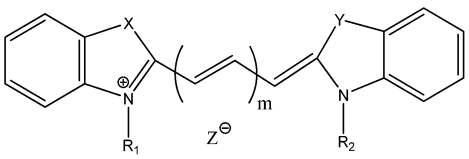

Scheme 1 Generic structure of cyanine dyes, with $m = 0$, 1, 3, 5; R_1 and R_2 = H, alkyl, benzyl groups; X and Y = N, O, P, S; Z = I, ClO_4, Cl.

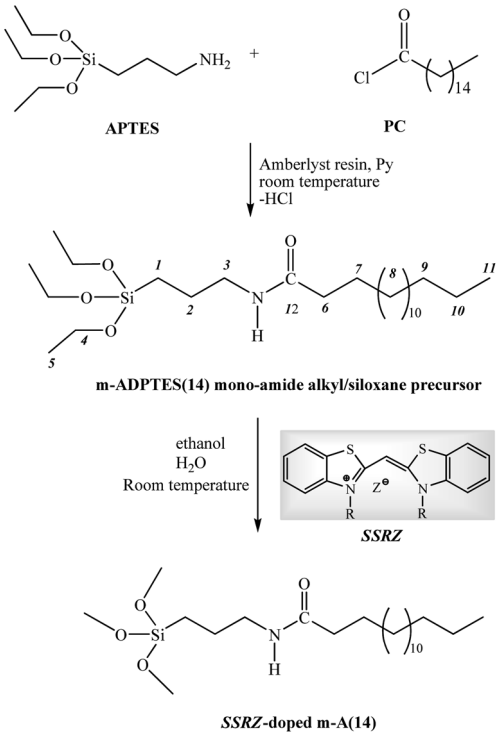

Scheme 2 Synthetic procedure of the m-A(14)$_n$***SSRZ*** mono-amidosils, with R = CH_3, C_2H_5 and $CH_2(C_6H_5)$ and Z = Cl, ClO_4 and I.

exhibited by the alkyl chains induces the emergence of a thermally actuated photoluminescence memory effect during heating–cooling cycles between 23 and 120 °C.[40]

The structure of the ***SSRZ***-doped mono-amidosils has been investigated in depth. The luminescence features of the chromophores in solution, in the solid state, as well as, encapsulated within the organic–inorganic hybrid structure have been also studied, in order to determine the effect of the solid host cage on the optical properties of the guest dyes.

Experimental section

Materials

Pyridine (Py, Panreac, 99.8%) and tetrahydrofuran (THF, Riedel-deHaen) were stored over molecular sieves. Amberlyst A-21 Ion-Exchange Resin (4.7 meq g^{-1}, Aldrich) was washed with THF and stored in an oven at 80 °C. 3-Aminopropyltriethoxysilane ($(CH_3CH_2O)_3Si(CH_2)_3NH_2$, APTES, Aldrich), palmitoyl chloride ($ClC(=O)-(CH_2)_{14}CH_3$, PC, Aldrich) and ethanol (CH_3CH_2OH, Fábrica de Álcool – Manuel Vieira e Ca. (Irmão) Sucrs, Lda, 99.9%) were used as received. High purity distilled water (H_2O) was used in all experiments. The monomethinecyanines employed were prepared according to the method reported elsewhere.[51–53]

Synthetic procedure

The mono-amide alkyl–siloxane precursor was prepared according to the method described in detail previously.[40] The first stage of the synthetic procedure involved the formation of an amide cross-link between the –Cl group of PC and the NH_2

group of APTES in the presence of THF, Py and Amberlyst A-21 Ion-Exchange Resin to yield the organic–inorganic hybrid precursor designated as mono-amidepropyltriethoxysilane ($(CH_3CH_2O)_3$–Si–$(CH_2)_3$–NH–C(=O)–$(CH_2)_{14}$–CH_3, m-ADPTES-(14)) (molar proportion APTES : PC : Amberlyst resin : Py = 1 : 1 : 1.2 : 0.2) (Scheme 2). This solution was stirred overnight at room temperature. The grafting process was infrared monitored: the intensity of the band attributed to the stretching vibration of the C=O group of the chloride acid, located at 1796 cm^{-1} in the spectrum of PC, was progressively reduced, until it disappeared upon completion of the reaction. In parallel, a series of new bands, associated with the characteristic vibrations of the amide group, appeared in the 1760–1530 cm^{-1} spectral interval. In the second stage of the synthetic procedure, a mixture of CH_3CH_2OH and H_2O ($Si : CH_3CH_2OH = 1 : 4$; $Si : H_2O = 1 : 1.5$) was added to m-ADPTES(14) to promote the hydrolysis and condensation reactions characteristic of the sol–gel process, followed by the incorporation of the monomethinecyanine ***SSRZ*** (Scheme 2). The resulting mixture was stirred in a sealed flask for 30 min and then cast to a Teflon mould, which was covered with Parafilm and left in a fume cupboard for 24 h. The mould was then transferred to an oven at 50 °C and the sample was aged for a period of one week. The ***SSRZ***-doped m-A(14) hybrid materials were produced as white powders. The doped samples have been represented by the notation m-A(14)$_n$***SSRZ***, where n, composition, is the molar ratio of amide (C=O) groups per ***SSRZ*** monomethinecyanine. A dilute sample ($n = 100$) and a concentrated one ($n = 20$) were prepared when the doping procedure involved the $SSC_2H_5ClO_4$ and $SSCH_2(C_6H_5)I$ monomethinecyanines. A single sample, with an intermediate composition ($n = 40$), was synthesized when the lower molecular weight $SSCH_3Cl$ compound was incorporated. Additional details of the synthesis have been collected in Table 1.

Methods

^{29}Si Magic Angle Spinning (MAS) and ^{13}C Cross Polarization (CP)/MAS Nuclear Magnetic Resonance (NMR) spectra were recorded on a Bruker Avance 400 (9.4 T) spectrometer at 79.49 and 100.62 MHz, respectively. ^{29}Si MAS NMR spectra were recorded with 2 μs ($\theta \approx 30°$) rf pulses, and recycle delay of 60 s and at a spinning rate of 5.0 kHz. ^{13}C CP/MAS NMR spectra were recorded with 4 μs ^1H 90° pulse, 2 ms contact time, a recycle delay of 4 s and at a spinning rate of 8 kHz. The chemical shifts (δ) are quoted in ppm from tetramethylsilane (TMS).

The X-ray diffraction (XRD) patterns were recorded with a Philips X'Pert MPD powder X-ray diffractometer, monochromated CuK_α radiation ($\lambda = 1.54$ Å) over a q ($q = 4\pi \sin\theta/\lambda$, 2θ being the scattering angle) range between 0.77 and 25 nm^{-1}.

Differential Scanning Calorimetry (DSC) measurements were obtained with a DSC131 Setaram differential scanning calorimeter. A mass of 5–10 mg was placed in 40 μL aluminum cans and stored in a desiccator over phosphorous pentoxide (P_2O_5) for one week at room temperature under vacuum. After the drying treatment the cans were hermetically sealed and the thermograms were recorded. Each sample was heated from 20 to 130 °C at 10 °C min^{-1}. The purge gas used in all experiments was high purity nitrogen (N_2) supplied at a constant flow rate of 35 cm^3 min^{-1}.

Scanning electron microscopy (SEM) images were obtained at 20 kV on a Hitachi Field Emission S-2700 microscope. SEM images were obtained at low vacuum. The sample was coated with gold.

Polarized Optical Microscopy (POM) images were recorded using an OPTIKA B-600POL microscope equipped with a 8 Mpixel digital Photo Camera. The images were analyzed using OPTIKA Vision Pro software.

Atomic Force Microscopy (AFM) images were recorded in a Veeco Metrology Multimode/Nanoscope IVA equipment (CEMUP-Porto contract REEQ/1062/CTM/2005), in tapping mode using a super sharp silicon tip, with a curvature radius of 10 nm, and frequency resonance of ≈300 kHz. Flattening and elimination of line noise tools and a low-pass filter provided by WSXM software[54] were used to improve the quality of the images.

Attenuated Total Reflectance (ATR) IR spectra were collected on a Thermoscientific Nicolet iS10: smart iTR, equipped with a diamond ATR crystal. For ATR data acquisition, a mass of

Table 1 Details of the synthesis of the m-A(14)$_n$***SSRZ*** mono-amidosils

First step – synthesis of the m-ADPTES(14) precursor[40]					
PC	APTES	Amberlyst A-21 Ion-Exchange Resin		Py	THF
1.00 mL (3.30 mmol)	774 μL (3.30 mmol)	0.841 g (3.90 mmol)		50 μL (0.660 mmol)	20 mL

Second step – synthesis of the m-A(14)$_n$*SSRZ* hybrids					
	$SSCH_3Cl$ (MM = 346.90 g mol^{-1})	$SSC_2H_5ClO_4$ (MM = 438.95 g mol^{-1})		$SSCH_2(C_6H_5)I$ (MM = 590.54 g mol^{-1})	
n	40	20	100	20	100
SSRZ	0.0285 g (0.0825 mmol)	0.0723 g (0.165 mmol)	0.0144 g (0.033 mmol)	0.0973 g (0.165 mmol)	0.0195 g (0.033 mmol)
CH_3CH_2OH	700 μL (13.20 mmol)	700 μL (13.20 mmol)		700 μL (13.20 mmol)	
H_2O	118 μL (6.60 mmol)	118 μL (6.60 mmol)		118 μL (6.60 mmol)	

approximately 2 mg of the sample was placed onto the crystal and the spectrum was recorded. An air spectrum was used as a reference in absorbance calculations. The sample spectra were collected at room temperature in the 4000–400 cm^{-1} range by averaging 64 scans at a spectral resolution of 2 cm^{-1}.

The Fourier Transform Raman (FT-Raman) spectra were recorded at room temperature with a Bruker Spectrometer, Model RFS100/S and the laser radiation emitted by a Nd:YAG laser with a wavelength of 1064 nm. The spectra were collected over the 4000–50 cm^{-1} range by averaging 400 scans at a spectral resolution of 4 cm^{-1} and using a 300 mW laser power.

To evaluate complex band ATR-IR and FT-Raman envelopes and to identify underlying spectral components, the iterative least-squares curve-fitting procedure in PeakFit software (version 4)[55] was used extensively throughout this study. The best fit of the experimental data was obtained by varying the frequency, bandwidth and intensity of the bands. Because of the morphology of materials under investigation, we employed Lorentzian band functions.

The UV–Vis absorption spectra of both ***SSRZ*** monomethinecyanines were measured by a double beam Thermo-Fischer Scientific spectrophotometer (model Evolution 160) within a wavelength range between 300 and 600 nm, using 1 cm thick vats and ethanol as solvent. The ethanolic solutions of the ***SSRZ*** have the concentration of 2×10^{-5} M.

The photoluminescence spectra were recorded at room temperature and at 12 K with a modular double grating excitation spectrofluorimeter with a TRIAX 320 emission monochromator (Fluorolog-3, Horiba Scientific) coupled to a R928 Hamamatsu photomultiplier, using a front face acquisition mode. The excitation source was a 450 W Xe arc lamp. The emission spectra were corrected for detection and optical spectral response of the spectrofluorimeter and the excitation spectra were corrected for the spectral distribution of the lamp intensity using a photodiode reference detector.

Results and discussion

In the ^{29}Si MAS NMR spectra of the $SSCH_3Cl$- and $SSC_2H_5ClO_4$-doped mono-amidosils the resonances observed lie between −45 and −75 ppm (Fig. S1a† in ESI) and are assigned to three types of silicon sites[40,56] T^1 (CH_2–Si(OSi)$(OH)_2$) (−49 ppm), T^2 (CH_2–Si$(OSi)_2$(OH)) (−59 ppm) and T^3 (CH_2–Si$(OSi)_3$) (−67 ppm) (Table 2). The non-existence of the resonances characteristic of Q type environments[56] (SiO_4 units) in these spectra reveals that no cleavage of the silicon–carbon bonds occurred during the synthesis of the materials. No T^0 (CH_2–Si$(OH)_3$)[56,57] environments associated with residual trihydroxysilane moieties could be detected either in any of these samples. Based on the relative populations of the T^1, T^2 and T^3 environments, the polycondensation degree *c* calculated for the $SSCH_3Cl$- and $SSC_2H_5ClO_4$-doped m-A(14) samples was 80 and 72%, respectively (Table 2). The magnitude of *c* in the latter material, coincident with that deduced previously for m-A(14),[40] suggests the existence of a 2D siliceous network. The empirical formulae derived for $SSCH_3Cl$- and $SSC_2H_5ClO_4$-doped m-A(14)-based samples show that some hydroxyl groups persisted bonded to the silicon atoms (Table 2). In contrast with the above samples, in the ^{29}Si MAS NMR spectra of the $SSCH_2(C_6H_5)$I-doped m-A(14)-based materials with $n = 100$ and 20 a peak at −45.3 ppm (Fig. S1a† in ESI), characteristic of the occurrence of T^0 sites,[57] was evident. This finding indicated that this monomethinecyanine inhibited condensation probably as a result of the steric hindrance caused by the bulky phenyl group. For this reason these two samples were discarded from the present study.

Table 2 ^{29}Si MAS and ^{13}C CP/MAS NMR data of selected m-A(14)$_n$***SSRZ*** mono-amidosils. Notes: T^1: (R–Si(OSi)$(OR)_2$; T^2 (R–Si$(OSi)_2$(OR) and T^3 (R–Si$(OSi)_3$[a]

^{29}Si MAS NMR			
δ (ppm)			
Non-doped	$SSCH_3Cl$	$SSC_2H_5ClO_4$	
∞	40	100	Attribution[40,56]
−49.5	−49.6	−49.8	T^1
−57.8	−60.5	−57.9	T^2
−67.0	−67.4	−65.8	T^3
74	80	72	*c*[b]
R′Si$(OH)_{1.1}(O)_{0.8}$	R′Si$(OH)_{1.2}(O)_{0.6}$	R′Si$(OH)_{0.8}(O)_{1.1}$	Empirical formula
^{13}C CP/MAS NMR			
δ (ppm)			
Non-doped	$SSCH_3Cl$	$SSC_2H_5ClO_4$	
∞	40	100	Attribution[40,58–61]
174	173.7	173.9	C^{12}
42	43.3	42.6	C^3
36	36.2	36.2	C^6
34	33.8	34.0	C^9
32	32.5	32.8	C^8 *trans*
—	30.3	30.5	C^8 *gauche*
26	27.6	27.3	C^7
24	24.3	24.4	C^2/C^{10}
14	14.6	14.6	C^{11}
11	10.7	11.2	C^1

[a] *c* (polycondensation degree) = $1/3(\%T^1 + 2\%T^2 + 3\%T^3) \times 100$. [b] R′=$CH_3(CH_2)_{14}C(=O)NH–(CH_2)_3$.

^{13}C CP/MAS data have been used to characterize the structure of the m-A(14) mono-amidosils doped with ***SSRZ*** and also the conformational state of the alkyl chains. The ^{13}C CP/MAS spectra of the m-A(14)-based mono-amidosils doped with $SSCH_3Cl$ and $SSC_2H_5ClO_4$ are dominated by a peak centered around 32–33 ppm, due to the resonance of the C^8 carbon atoms of the alkyl chains (Fig. S1b† in ESI and Table 2), and characteristic of all-*trans*, zigzag, highly ordered alkyl chains.[59,62–64] In the ^{13}C CP/MAS spectra of m-A$(14)_{40}SSCH_3Cl$ and m-A$(14)_{100}SSC_2H_5ClO_4$ the 30 ppm resonance peak due to C^8 carbon atoms of alkyl chains in *gauche* conformations[62] is detected as a shoulder (Fig. S1b† in ESI), indicating that in the two materials analyzed the alkyl chains adopt essentially all-*trans* conformations. The peaks associated with the resonance of the CH_2 carbon atoms of the alkyl chains, of the Si-bonded

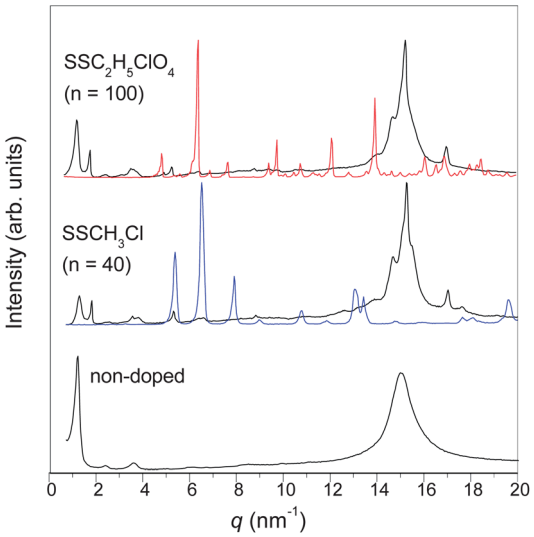

Fig. 1 XRD patterns of m-A(14),[40] of selected m-A(14)$_n$***SSRZ*** mono-amidosils (black lines) and of the corresponding free monomethinecyanines (red and blue lines).

propyl chains and of the amide carbonyl groups of m-A(14) are also discerned in these spectra (Fig. S1b† in ESI and Table 2), revealing that no cleavage of the functional groups of the precursor molecule (alkyl chains, propyl chains and amide cross-links) occurred during the second stage of the synthetic procedure. The ^{13}C CP/MAS results also demonstrate that the hydrolysis reaction was complete in the case of the $SSCH_3Cl$- and $SSC_2H_5ClO_4$-doped m-A(14) mono-amidosils (Fig. S1b† in ESI and Table 2), as indicated by the absence of the peaks associated with the resonance of the ethoxyl carbon atoms (C^4 and C^5).[40]

Comparison of the XRD patterns of the m-A(14)$_{40}SSCH_3Cl$ and m-A(14)$_{100}SSC_2H_5ClO_4$ mono-amidosils with those of $SSCH_3Cl$ (blue line in Fig. 1) and $SSC_2H_5ClO_4$ (red line in Fig. 1) allows concluding that in both samples the host hybrid structure was able to encapsulate efficiently the guest monomethinecyanines which were, therefore, not expelled from it.

In the low-q region ($q < 12$ nm^{-1}) of the XRD patterns of the $SSCH_3Cl$- and $SSC_2H_5ClO_4$-doped mono-amidosils the most prominent reflection is discerned at $q = 1.26$ nm^{-1} (Fig. 2a). This peak is the first of the n^{th}-order peaks of a lamellar structure (red vertical lines in Fig. 2a) with a spacing $d_1 = 4.99$ nm (where $d = n2\pi/q_n$). In addition these materials give rise to another reflection at $q = 1.83$ nm^{-1} which corresponds to the 1st reflection of a second lamellar structure (blue dotted vertical lines in Fig. 2a) characterized by a spacing $d_2 = 3.43$ nm. As the value of d_1 coincides with the interlamellar distance reported for m-A(14) (5.0 ± 0.2 nm),[40] it may be concluded that in both samples the lamellar structure of the m-A(14) matrix coexists with a new lamellar structure with lower spacing.

In the high-q region ($q > 12$ nm^{-1}) of the XRD patterns of the ***SSRZ***-doped m-A(14)-based mono-amidosils a prominent broad peak centered near 15.2 nm^{-1} is seen (Fig. 2b). This peak is significantly better resolved than that of m-A(14), suggesting a higher degree of structural order in the doped samples. The peak contains three contributions (Fig. 2b): (1) a peak at about 14.7 nm^{-1} ($d_1 = 0.43$ nm) corresponding to amide–amide spacings;[40] (2) a peak at 15.2 nm^{-1} ($d_2 = 0.41$ nm) due to ordering within the 2D siliceous domains[65] and (3) peaks at 15.9 and 17.0 nm^{-1} ($d_3 = 0.39$ and 0.37 nm, respectively) assigned to chain–chain distances.[66,67] In addition, m-A(14)$_{40}SSCH_3Cl$ also gives rise to a peak at 17.7 nm^{-1} ($d_4 = 0.35$ nm) (Fig. 2b). The 15.9 nm^{-1} peak is associated with chains in *gauche* conformations, whereas the peaks at 17.0 and 17.7 nm^{-1} are associated with chains in all-*trans* conformations.[67,68] The shift to higher q of the m-A(14) peak related to all-*trans* chain–chain spacing demonstrates that the inclusion of the monomethinecyanines induces the decrease of the mean distance between the alkyl chains. In the case of the sample doped with the less bulky $SSCH_3Cl$ the effect is more marked and two different mean distances between the ordered alkyl chains occur. It is essential to emphasize that the three structural effects resulting from the incorporation of the methinecyanines into m-A(14) (*i.e.*, the emergence of a new lamellar ordered phase, the preservation of the original lamellar structure and the complete dissolution of the dye compounds) are indeed extraordinary, considering the

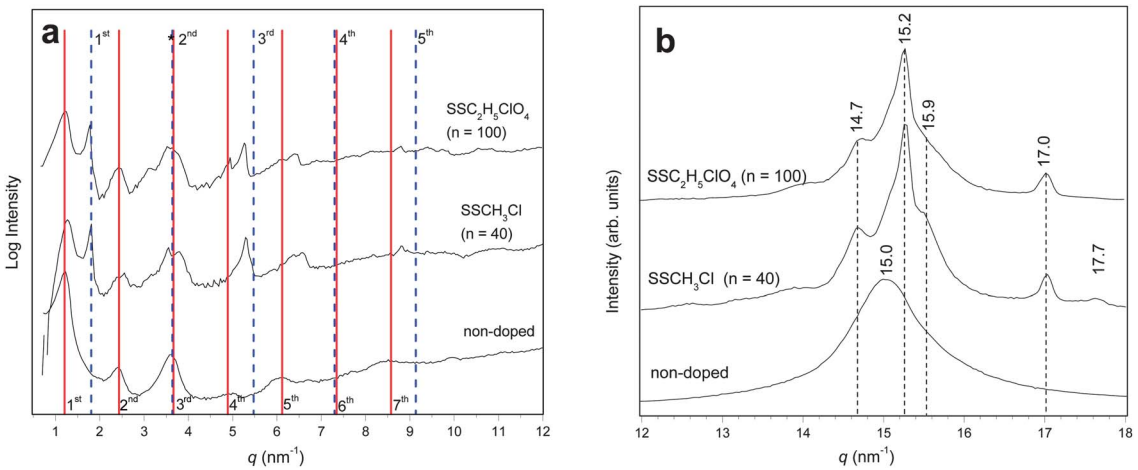

Fig. 2 XRD patterns of m-A(14)[40] and of selected m-A(14)$_n$***SSRZ*** mono-amidosils in the low-q (a) range and high-q (b) range.

size of $SSCH_3Cl$ and $SSC_2H_5ClO_4$. In fact similar structural manifestations were produced previously upon doping m-A(14) with europium triflate.[69] However, the volume occupied by this salt is significantly smaller than that occupied by the bulky, rigid monomethinecyanines. These findings strongly suggest that in the m-A(14)$_n$***SSRZ*** mono-amidosils $SSCH_3Cl$ and $SSC_2H_5ClO_4$ interact directly with the host matrix, yielding the new lamellar phase and inhibiting their own crystallization. This interaction will be discussed below.

In a previous work,[40] it was noted that the self-assembly forces of m-A(14) (hydrogen bonding between amide groups, van der Waals interactions between alkyl chains and an entropic term related to the phase separation between the alkyl chains and the siloxane nanodomains) determined the emergence of a thermally actuated photoluminescence memory effect induced by a reversible order–disorder phase transition of the alkyl chains. The characteristics of this thermal event are collected in Table 3. During the order–disorder transition, while most of the enthalpy change is associated with a large cohesive van der Waals energy contribution, the entropy change is not only associated with a volume expansion, but also with contributions related to the conformational state of the chains and with an excluded volume.[70]

The DSC curves of the ***SSRZ***-doped m-A(14)-based hybrids in the 20–130 °C range, represented in Fig. 3, show that the incorporation of the monomethinecyanines $SSCH_3Cl$ and $SSC_2H_5ClO_4$ into the m-A(14) framework affects drastically its thermal behavior. Instead of exhibiting a single endotherm, the DSC thermograms of m-A(14)$_{40}$$SSCH_3Cl$ and m-A(14)$_{100}$$SSC_2H_5ClO_4$ display three endotherms centered at *ca.* 53, 76/81 and 90/92 °C (Table 3).

On the basis of the XRD data, the 76/81 and 90/92 °C peaks are ascribed to the order–disorder phase transitions of the new lamellar phase formed in the presence of the monomethinecyanines and of the lamellar structure of m-A(14), respectively. These results lend support to the previous conclusion that doping induces a reduction of the phase transition temperature of the lamellar phase of m-A(14).[69] The origin of the endothermic peak at 53 °C is unknown.

The downshift of the peak temperature of the endotherm corresponding to the new lamellar structure formed in the doped samples with respect to that of the original lamellar structure of m-A(14) (from 106 to about 76 and 81 °C upon doping with $SSCH_3Cl$ and $SSC_2H_5ClO_4$, respectively, Table 3) and the significant reduction of the enthalpy and entropy changes measured in the case of m-A(14)$_{100}$$SSC_2H_5ClO_4$ (from 30.44 to 9.89 J g^{-1} and from 0.287 to 0.120 J g^{-1} °C^{-1}, respectively) (Table 3), provide strong evidence that the energetics of the melting of the alkyl chains of m-A(14) are deeply altered in the presence of the monomethinecyanines.

The SEM images of Fig. 4 show that m-A(14)$_{40}$$SSCH_3Cl$ and m-A(14)$_{20}$$SSC_2H_5ClO_4$ are composed of crystalline plates of nanometer thickness and micrometer lateral dimensions. However, while in the case of m-A(14)$_{40}$$SSCH_3Cl$ the plates are arranged along the same direction (Fig. 4a), in

Table 3 Thermal data of selected m-A(14)$_n$***SSRZ*** mono-amidosils

m-A(14)$_n$***SSRZ***	Parameter				
SSRZ	n	T_{onset} (°C)	T_{peak} (°C)	ΔH (J g^{-1})	ΔS (J g^{-1} °C^{-1})
Non-doped	∞	96	106	30.44	0.287
$SSCH_3Cl$	40	—	90	—	—
		72	76	—	—
		42	53	13.09	0.250
$SSC_2H_5ClO_4$	100	87	92	3.94	0.043
		75	81	9.89	0.120
		42	53	23.61	0.450

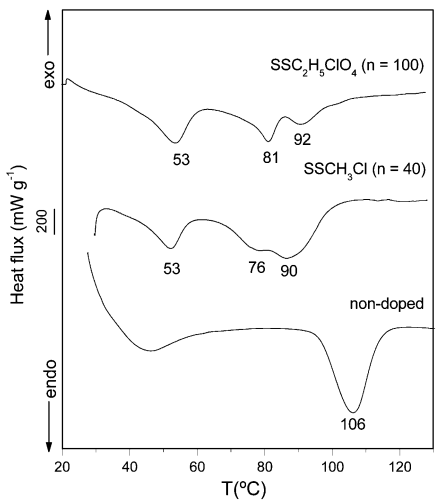

Fig. 3 DSC curves of m-A(14)[40] and of selected m-A(14)$_n$***SSRZ*** mono-amidosils.

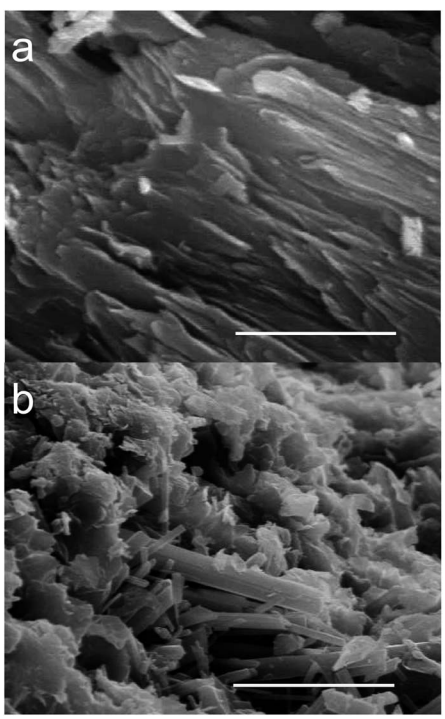

Fig. 4 SEM images of the m-A(14)$_{40}$$SSCH_3Cl$ (a, bar scale = 5 μm) and m-A(14)$_{20}$$SSC_2H_5ClO_4$ (b, bar scale = 20 μm) mono-amidosils.

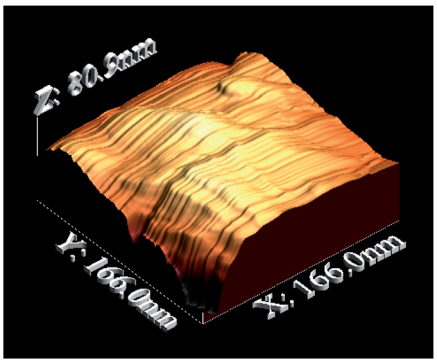

Fig. 5 3D-AFM topographic image of the m-A(14)$_{20}$SSC$_2$H$_5$ClO$_4$ mono-amidosil.

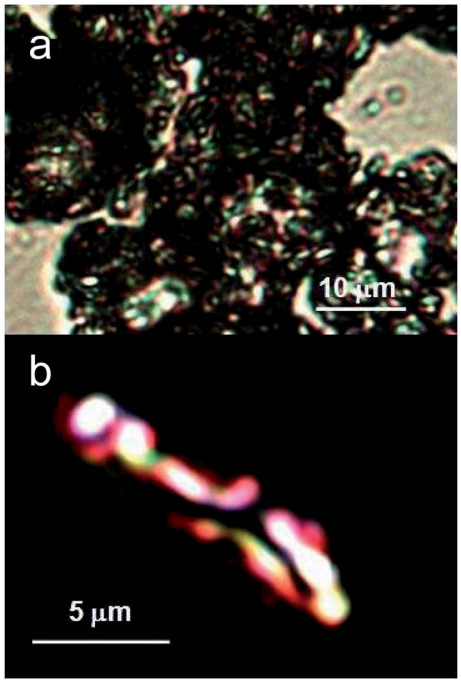

Fig. 6 POM images of m-A(14)$_{20}$SSC$_2$H$_5$ClO$_4$ mono-amidosil recorded between parallel (a) and crossed (b) polarizers.

m-A(14)$_{20}$SSC$_2$H$_5$ClO$_4$ the plates are randomly distributed (Fig. 4b). In addition, in the latter compound micro-objects with parallelopiped shape emerge (Fig. 4b). The lamellar arrangement of the m-A(14)$_{20}$SSC$_2$H$_5$ClO$_4$ mono-amidosil is clearly observed in the 3D-AFM image of Fig. 5. The birefringence detected in the POM images of this sample (Fig. 6) suggests the existence of anisotropy at the submicrometer scale.

Information on the *trans*/*gauche* conformer ratio, chain packing and the intermolecular interactions between the alkyl chains of the m-A(14)$_n$***SSRZ*** mono-amidosils was obtained from the inspection of the FT-IR and FT-Raman symmetric and asymmetric CH$_2$ stretching modes (ν_sCH$_2$ and ν_aCH$_2$, respectively)[71–77] and of the FT-Raman C–C skeletal stretching (νC–C) mode.[78]

In the FT-IR ν_aCH$_2$ and ν_sCH$_2$ regions m-A(14)$_{40}$SSCH$_3$Cl and m-A(14)$_{100}$SSC$_2$H$_5$ClO$_4$ produce two medium intensity features at 2915 cm and 2848 cm^{-1} (Fig. 7a), a proof that the alkyl chains are essentially fully stretched (all-*trans* conformations) and densely packed in the monomethinecyanines-doped m-A(14)-based mono-amidosils analysed.[71–75] Interestingly, these bands are downshifted with respect to those of the m-A(14) matrix (2920 and 2850 cm^{-1}, respectively),[40] a result that may be correlated with an increase in the conformational order of the alkyl chains upon doping.

In the FT-Raman νCH$_2$ region of the non-doped[40] and ***SSRZ***-doped m-A(14) mono-amidosils the ν_aCH$_2$ and ν_sCH$_2$ bands observed at 2881 cm^{-1} (νS) and 2844 cm^{-1} (S) (Fig. 7b), respectively, are characteristic of crystalline, fully stretched and highly packed alkyl chains (all-*trans* conformers).[71,74,75] Another band that gives support to this conclusion is that at *ca.* 2934 cm^{-1}, attributed to the ν_sCH$_2$ fundamental and to the Fermi resonance between the ν_sCH$_2$ fundamental and the many overtones of the δCH$_2$ vibrations.[71,73–75] The values of the intensity ratio *r* (where *r* is Iν_aCH$_2$/Iν_sCH$_2$) calculated for m-A(14)$_{100}$SSCH$_3$Cl and m-A(14)$_{100}$SSC$_2$H$_5$ClO$_4$ were 1.59 and 1.50, respectively. The value deduced for the former material is practically coincident with that reported for m-A(14) (1.60),[40] demonstrating that in the presence of SSCH$_3$Cl virtually all the alkyl chains of m-A(14) adopt all-*trans* conformations. In m-A(14)$_{100}$SSC$_2$H$_5$ClO$_4$ a minor proportion of *gauche* conformers co-exists with the *trans* conformers.[79]

In the νC–C region the FT-Raman spectral signature of the m-A(14)$_{40}$SSCH$_3$Cl and m-A(14)$_{100}$SSC$_2$H$_5$ClO$_4$ mono-amidosils resembles closely that of m-A(14)[40] (Fig. 8). The three samples give rise to the typical bands of all-*trans* conformers at 1127 and 1061 cm^{-1}, but not the characteristic band of the interruption of all-*trans* conformations at 1080 cm^{-1}.[78]

To determine the spectral consequences arising from the inclusion of SSCH$_3$Cl and SSC$_2$H$_5$ClO$_4$ into m-A(14), two characteristic bands of the amide cross-links were inspected: the amide I and amide II bands. The amide I mode, which receives a major contribution of the C=O stretching vibration, is sensitive to the specificity and magnitude of hydrogen bonding. Usually the amide I band consists of several distinct components corresponding to different environments of the C=O groups.[80,81] The involvement of C=O groups in hydrogen bonding interactions results in a shift of the amide I band of the non-bonded C=O group to lower wavenumbers.[80,81] The amide II mode, essentially associated with the N–H in-plane bending vibration, is sensitive to chain conformation and intermolecular hydrogen bonding, providing useful information about the distribution of hydrogen bond strengths.[80] When the C=O group is included in hydrogen-bonded aggregates, the amide II band emerges at a higher wavenumber than in the case of the free C=O group.

The strength of the hydrogen bonded array formed by the amide groups in the m-A(14)$_{40}$SSCH$_3$Cl, m-A(14)$_{100}$SSC$_2$H$_5$ClO$_4$ and m-A(14)$_{20}$SSC$_2$H$_5$ClO$_4$ mono-amidosils was primarily deduced from the wavenumber difference ($\Delta\bar{\nu}$) between the intensity maxima of the amide I and amide II bands. In the three samples the amide I and amide II regions are dominated by a sharp band at 1639 cm^{-1} and by a less intense and broader band at 1549 cm^{-1} (Fig. S2† in ESI). The $\Delta\bar{\nu}$ calculated (90 cm^{-1})

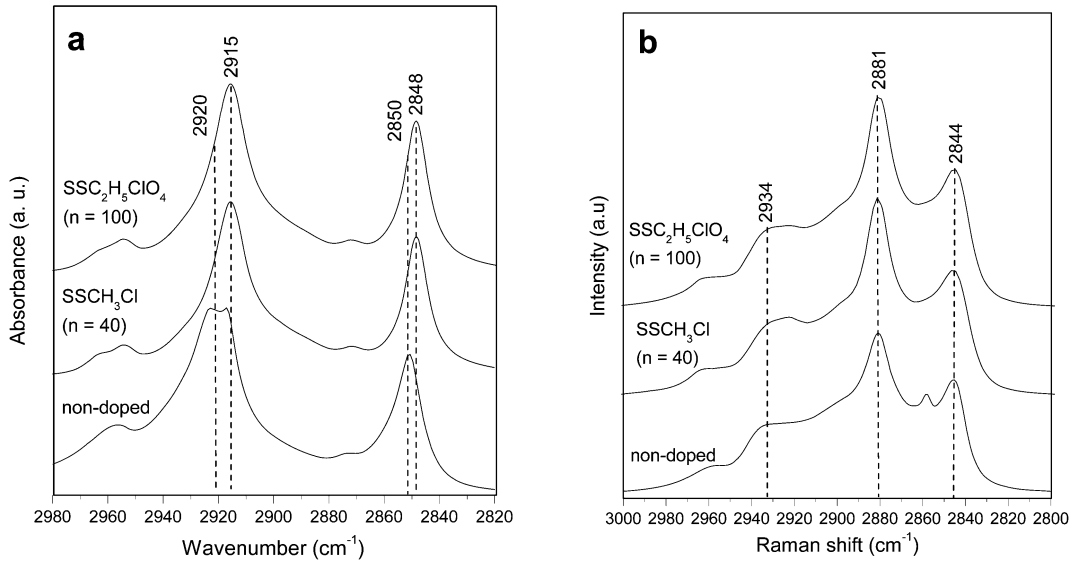

Fig. 7 FT-IR (a) and FT-Raman (b) spectra of m-A(14)[40] and of selected m-A(14)$_n$***SSRZ*** mono-amidosils in the $\nu_a CH_2$ and $\nu_s CH_2$ regions.

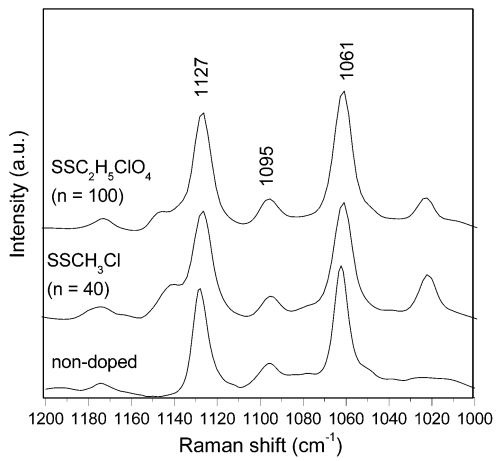

Fig. 8 FT-Raman spectra of m-A(14)[40] and of the m-A(14)$_n$***SSRZ*** mono-amidosils in the νC–C region.

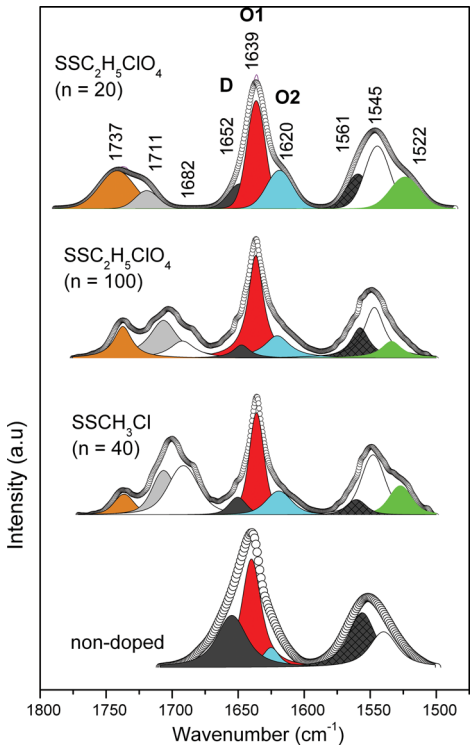

Fig. 9 Results of the curve fitting performed in the amide I and amide II regions of the FT-IR spectra of m-A(14)[40] and of the m-A(14)$_n$***SSRZ*** mono-amidosils.

coincides with that of m-A(14) (92 cm^{-1}),[40] clearly suggesting that globally the strength of the hydrogen bonded aggregates formed in pristine m-A(14) was not affected by the addition of the monomethinecyanines.

The amide I band of the three doped mono-amidosils was decomposed into six components situated at 1737, 1711, 1682, 1652, 1639 and 1620 cm^{-1} (Fig. 9 and Table S1† in ESI). The band at 1682 cm^{-1} is attributed to "free" C═O groups (F),[40,81] whereas the band at 1652 cm^{-1} is ascribed to hydrogen-bonded C═O groups in disordered amide–amide aggregates (aggregate D).[40,81] The events at 1639 and 1620 cm^{-1} are assigned to hydrogen-bonded C═O groups in ordered amide–amide aggregates of increasing strength (aggregates O1 and O2, respectively).[40,81] The amide II of the same samples was decomposed into three components located at approximately 1561, 1545 and 1522 cm^{-1} (Fig. 9 and Table S1† in ESI). This suggests that in the m-A(14)$_n$***SSRZ*** mono-amidosils hydrogen-bonded aggregates with at least three distinct degrees of order exist, a situation similar to that found in m-A(14).[40]

Analysis of the graph in Fig. 10 allows concluding that the most relevant consequences resulting from the inclusion of the $SSC_2H_5ClO_4$ into the m-A(14) host matrix ($n = 100$) are a drastic breakdown of aggregates D and O1, the growth of two new components at 1739 and 1711 cm^{-1} and a slight increase of the proportion of O2 aggregates. Upon increasing the

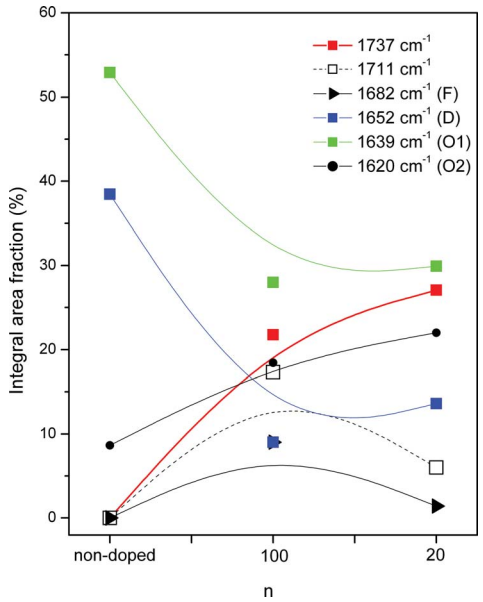

Fig. 10 Composition dependence of the integral area fraction of the different spectral components resolved in the amide I region of m-A(14)[40] and the m-A(14)$_n$SSC$_2$H$_5$ClO$_4$ mono-amidosils. The lines drawn are just guides for the eyes.

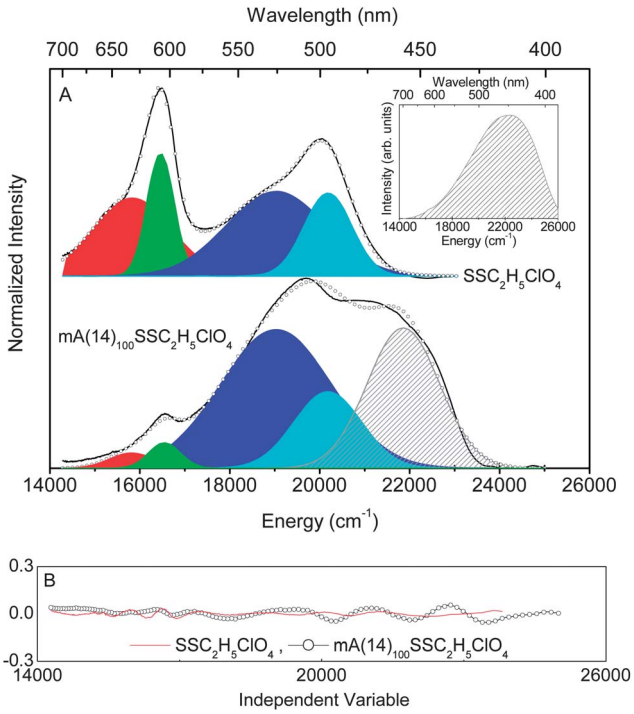

Fig. 11 (A) Emission spectra of SSC$_2$H$_5$ClO$_4$ and m-A(14)$_{100}$SSC$_2$H$_5$ClO$_4$ excited at 360 and 380 nm, respectively. The Gaussian fit components (shadow areas) and the cumulative fit (open circles) are also shown. The inset shows the emission spectrum of the pristine m-A(14)[40] excited at 360 nm. (B) Regular residual plots ($\chi^2_{red} < 10^{-5}$) are also shown for a better judgment of the fit quality.

monomethinecyanine concentration, these trends become more marked. The fraction of "free" C=O groups remains practically unchanged.

The new bands which emerge at about 1737 and 1711 cm^{-1}, independently of the methinecyanine incorporated and its concentration (Fig. 9), are tentatively attributed to the formation of new hydrogen bonded aggregates, probably involving the interaction of the amide C=O groups of m-A(14) with the S atoms of the monomethinecyanines.[82] The presence of a weak "free" band in the amide I region of the doped mono-amidosils (Fig. 9) suggests that the monomethinecyanine–matrix coordination process which causes a major destruction of the hydrogen-bonded aggregates D and O1 leads in parallel to the release of a few C=O groups. These spectral findings confirm the conclusion retrieved from XRD and DSC data that in the m-A(14)$_n$***SSRZ*** mono-amidosils the monomethinecyanines are bound to the host m-A(14) matrix. This interaction is presumably responsible, not only for the complete dissolution of the monomethinecyanine compounds, but also for the formation of the new lamellar phase. In the latter process, it is therefore clear that the amide C=O groups play a key-role.

The emission spectrum of m-A(14)$_{100}$SSC$_2$H$_5$ClO$_4$ is well reproduced by a sum of five Gaussian functions corresponding to the superposition of four monomethinecyanine components (high-wavelength region, Fig. 11 and Table S2† in ESI) with the broad band of pristine m-A(14) mono-amidosil (inset in Fig. 11).[40]

Whilst the emission features, namely energy and full-width-at-half-maximum (*fwhm*) for the pure monomethinecyanine are independent of the excitation wavelength in the 270–440 nm interval (Fig. S3† in ESI), the spectrum of m-A(14)$_{100}$SSC$_2$H$_5$ClO$_4$ displays marked changes (Fig. S4† in ESI). In particular, a variation in the relative intensity of the emission components and a deviation of the maximum peak position towards the red are observed as the excitation wavelength increases (Fig. S4† in ESI). These changes are ascribed to the contribution of the hybrid host intrinsic emission, previously attributed to the convolution of electron–hole recombinations that occur within the amide cross-linkages and within oxygen-related defects found in the siliceous skeleton.[40] The energy dependence on the excitation wavelength was observed for similar hybrid materials, being assigned to recombination involving localized states.[83]

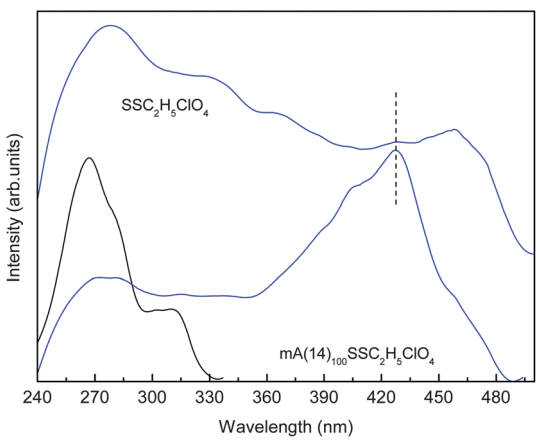

Fig. 12 Excitation spectra of the monomethinecyanine SSC$_2$H$_5$ClO$_4$ and of the m-A(14)$_{100}$SSC$_2$H$_5$ClO$_4$ mono-amidosil monitored at 440 nm (black line) and at 530 nm (blue line).

The presence of different monomethinecyanine components in the emission spectra of $SSC_2H_5ClO_4$ and m-A(14)$_{100}SSC_2H_5ClO_4$ points out the formation of monomethinecyanine aggregates in the solid state. The non-aggregated form is responsible for the absorption peak at *ca.* 421 nm detected in the absorption spectrum of a diluted solution of the dye (Fig. S5† in ESI). Therefore, we suggest the formation of fluorescent J-dimers in the solid state, as the emission spectra is red-shifted relatively to the absorption energy of the non-aggregated form.[39]

The distinct nature of the emission components is supported by the analysis of the excitation spectra monitored at distinct wavelengths (Fig. 12, S6 and S7† in ESI). While the excitation spectrum of $SSC_2H_5ClO_4$ is independent of the monitoring wavelength (425–650 nm), the spectrum of m-A(14)$_{100}SSC_2H_5ClO_4$ depends on it, corroborating the presence of mono-amidosil emission components of different origin. The spectra of the monomethinecyanine displays a large band between 240 and 510 nm with two main components at 280 and 450 nm. The excitation spectrum of the doped-mono-amidosil monitored within the hybrid host intrinsic emission (440 nm) shows two distinct components at 268 and 315 nm, whereas the spectrum monitored within the monomethinecyanine related component (530 nm), apart from an inversion in the relative intensity displays the same components detected for $SC_2H_5ClO_4$ together with a component at *ca.* 430 nm (not detected in the excitation spectra of the monomethinecyanine and marked with a dashed line in Fig. 12). This observation suggests the occurrence of energy transfer involving the hybrid excited states and the monomethinecyanine levels.

Conclusions

In the present work we have investigated mono-amide cross-linked alkyl–siloxane hybrids, designated as mono-amidosils, incorporating three monomethinecyanines noted as ***SSRZ*** ($SSCH_3Cl$, $SSC_2H_5ClO_4$ and $SSCH_2(C_6H_5)I$). The doped samples have been represented by the notation m-A(14)$_n$***SSRZ***, where *n* is the molar ratio of amide (C=O) groups per ***SSRZ***. In the presence of the bulky $SSCH_2(C_6H_5)I$ dye the condensation of the siloxane network was incomplete. In contrast the addition of $SSCH_3Cl$ and $SSC_2H_5ClO_4$ was successful, yielding materials in which the original lamellar structure of m-A(14) and a new lamellar phase with lower spacing emerged and in which the crystallisation of the monomethinecyanine compounds was inhibited. The addition of $SSCH_3Cl$ and $SSC_2H_5ClO_4$ to m-A(14) led to the decrease of the mean distance between the all-*trans* alkyl chains. In the presence of the less bulky $SSCH_3Cl$ two different mean distances between the ordered alkyl chains were detected. The complete dissolution of the monomethinecyanine compounds within the host matrix and the formation of the new lamellar structure have been ascribed to monomethinecyanines–matrix coordination *via* bonding of the S atom of the dye compounds to the amide C=O group of m-A(14). This interaction, which, implied a major destruction of the disordered and ordered hydrogen-bonded aggregates of m-A(14), did not affect globally the strength of its hydrogen-bonded array. The m-A(14)$_{100}SSC_2H_5ClO_4$ displays room temperature emission in the visible spectral region (380–680 nm) due to the convolution of the hybrid host intrinsic emission (blue spectral region) with that of the dye (green and red spectral regions) ascribed to the formation of fluorescent J-dimers. The analysis of the excitation spectra (monitored along the emission spectra) evidences the presence of host-to-monomethinecyanine energy transfer.

Acknowledgements

This work was supported by Fundação para a Ciência e a Tecnologia (FCT) and FEDER (contracts PTDC/CTM/101324/2008, PTDC/QUI-QUI/100896/2008, Pest-14C/CTM/LA0011/2011 and Pest-C/SAU/UI0709/2011). S. C. Nunes and C. B. Ferreira acknowledge FCT for grants (SFRH/BPD/63152/2009 and BIC/PEst-C/QUI/UI0616/2011, respectively). J. Hümmer, a student of Technology of Functional Materials at the Julius-Maximilian-University in Würzburg (Germany), was involved in this work in the framework of an internship at the Department of Chemistry of UTAD, Vila Real, from September to October 2010. The authors thank Dr. Raquel Rosa, of the Communication and Image Office of the University of Beira Interior (Portugal) for the Cover artwork.

Notes and references

1 C. Sanchez and P. Gomez Romero, *Functional Hybrid Materials*, Wiley Interscience, New York, 2003.
2 G. Kickelbick, *Hybrid materials: synthesis, characterization and applications*, Wiley-VCH, Weinheim, 2007.
3 D. A. Loy and K. J. Shea, *Chem. Rev.*, 1995, **95**(5), 1431–1432.
4 J. D. Mackenzie, *J. Sol-Gel Sci. Technol.*, 1994, **2**(1–3), 81–86.
5 C. Sanchez and F. Ribot, *New J. Chem.*, 1994, **18**, 1007–1047.
6 C. J. Brinker and G. W. Scherer, *Sol–Gel Science, The Physics and Chemistry of Sol–Gel Processing*, Academic Press, San Diego, CA, 1990.
7 C. Sanchez, B. Julián, P. Belleville and M. Popall, *J. Mater. Chem.*, 2005, **15**, 3559–3592.
8 L. D. Carlos, R. A. S. Ferreira, V. de Zea Bermudez and S. J. L. Ribeiro, *Adv. Mater.*, 2009, **21**(5), 509–534.
9 B. Lebeau, N. Herlet, J. Livage and S. Sanchez, *Chem. Phys. Lett.*, 1993, **206**, 15–20.
10 B. Lebeau and P. Innocenzi, *Chem. Soc. Rev.*, 2011, **40**, 886–906.
11 B. Dunn, F. Nishida, A. Toda, J. I. Zink, T. Allik, S. Chandra and J. Hutchinson, *Mater. Res. Soc. Symp. Proc.*, 1994, **329**, 267–277.
12 F. Del Monte and D. Levy, *Chem. Mater.*, 1995, **7**, 292–298.
13 F. del Monte and D. Levy, *J. Phys. Chem. B*, 1998, **102**, 8036–8041.
14 M. L. Ferrer, F. del Monte and D. Levy, *Langmuir*, 2003, **19**, 2782–2786.
15 V. Deshpande and U. Kumar, *J. Lumin.*, 2008, **128**, 1121–1131.
16 A. V. Deshpande and U. Kumar, *J. Lumin.*, 2010, **130**, 839–844.

17 R. Reisfeld, A. Weiss, T. Saraidarov, E. Yariv and A. A. Ishchenko, *Polym. Adv. Technol.*, 2004, **15**, 291–301.
18 P. Prosposito, M. Casalboni, F. de Matteis, A. Quatela, M. Glasbeek, E. Van Veldhoven and H. Zhang, *J. Sol-Gel Sci. Technol.*, 2003, **26**, 909–913.
19 F. Wang, W. B. Tan, Y. Zhang, X. Fan and M. Wang, *Nanotechnology*, 2006, **17**, R1–R13.
20 I. Miletto, A. Gilardino, P. Zamburlin, S. Dalmazzo, D. Lovisolo, G. Caputo, G. Viscardi and G. Martra, *Dyes Pigm.*, 2010, **84**, 121–127.
21 L. Wang, K. Wang, S. Santra, X. Zhao, L. Hilliard, J. Smith, Y. Wu and W. Tan, *Anal. Chem.*, 2006, **78**, 646–654.
22 G. Schulz-Ekloff, D. Wohrle, B. van Duffel and R. A. Schoonheydt, *Microporous Mesoporous Mater.*, 2002, **51**, 91–138.
23 G. Shottner, *Chem. Mater.*, 2001, **13**, 3422–3435.
24 M. Jung Choi, T. Smoother, A. A. Martin, A. M. McDonagh, P. J. Maynard, C. Lennard and C. Roux, *Forensic Sci. Int.*, 2007, **173**, 154–160.
25 J. Bujdák, *Appl. Clay Sci.*, 2006, **34**, 58–73.
26 D. Avnir, D. Levy and R. Reisfeld, *J. Phys. Chem.*, 1984, **88**, 5956–5959.
27 E. Yariv, S. Schultheiss, T. Saraidarov and R. Reisfeld, *Opt. Mater.*, 2001, **16**, 29–38.
28 S. Schultheiss, E. Yariv, R. Reisfeld and H. Dieterbreuer, *Photochem. Photobiol. Sci.*, 2002, **1**(5), 320–323.
29 T. Seçkin, A. Gultek and S. Kartaca, *Dyes Pigm.*, 2003, **56**, 51–57.
30 M. T. Laranjo, V. Stefani, E. V. Benvenutti, T. M. M. Costa, G. O. Ramminger and M. R. Gallas, *J. Non-Cryst. Solids*, 2007, **353**, 24–30.
31 J. Tu, N. Li, Y. Chi, S. Qu, C. Wang, Q. Yuan, X. Li and S. Qiu, *Mater. Chem. Phys.*, 2009, **118**, 273–276.
32 C. M. Carbonaro, *J. Photochem. Photobiol., A*, 2011, **222**, 56–63.
33 C. M. Carbonaro, P. C. Ricci, S. Grandi, M. Marceddu, R. Corpino, M. Salisa and A. Anedda, *RSC Adv.*, 2012, **2**, 1905–1912.
34 I. Miletto, E. Bottinelli, G. Caputo, S. Coluccia and E. Gianotti, *Phys. Chem. Chem. Phys.*, 2012, **14**, 10015–10021.
35 R. Reisfeld, *Opt. Mater.*, 2001, **16**, 1–7.
36 H. Hirashima, H. Imai and Y. Fuki, *J. Sol-Gel Sci. Technol.*, 2003, **26**, 383–388.
37 J. I. Zink and B. Dunn, in *Sol–Gel Optics, Processing and Applications*, ed. L. Klein, Kluwer Academic Publishers, Dordrecht, 1994, 303.
38 B. Dunn and J. I. Zink, *J. Mater. Chem.*, 1991, **1**, 903–913.
39 V. V. Egorov, *Phys. Procedia*, 2009, **2**, 223–326.
40 L. D. Carlos, V. de Zea Bermudez, V. S. Amaral, S. C. Nunes, N. J. O. Silva, R. A. S. Ferreira, C. V. Santilli, D. Ostrovskii and J. Rocha, *Adv. Mater.*, 2007, **19**, 341–348.
41 A. Fukuoka, H. Miyata and K. Kuroda, *Chem. Commun.*, 2003, 284–285.
42 B. Lebeau, C. E. Fowler, S. Mann, C. Farcet, B. Charleaux and C. Sanchez, *J. Mater. Chem.*, 2000, **10**, 2105–2108.
43 B. Lebeau, C. E. Fowler, S. R. Hall and S. Mann, *J. Mater. Chem.*, 1999, **9**, 2279–2281.
44 B. Lebeau, J. Patarin and C. Sanchez, *Azo Journal of Materials Online*, 2005, **1**, 1–2.
45 H. Zollinger, *Color Chemistry*, VCH, Weinheim, 1988.
46 M. Matsuoka, *Infrared Absorbing Dyes*, Plenum Press, New York, 1990.
47 N. Tyutlkov, J. Fabian, A. Mehlhorn, F. Dietz and A. Tadjer, *Polymethine Dyes, Structure and Properties*, St. Kliment Ohridski University Press, Sofia, 1991.
48 A. Mishra, R. K. Behera, P. K. Behera, B. K. Mishra and G. B. Behera, *Chem. Rev.*, 2000, **100**, 1973–2011.
49 M. Panighahi, S. Dash, S. Patel and B. K. Mishra, *Tetrahedron*, 2012, **68**(3), 781–805.
50 P. J. Sims, A. S. Waggoner, C. H. Wang and J. F. Hoffman, *Biochemistry*, 1974, **13**, 3315–3340.
51 F. M. Hamer, in *The Cyanine Dyes and Related Compounds – The Chemistry of Heterocyclic Compounds*, ed. A. Weissberger, Interscience Publishers, New York, 1971, vol. 18.
52 K. Venkataraman, in *The Chemistry of Synthetic Dyes*, ed. L. F. Fieser and M. Fieser, Academic Press Inc., New York, 1952, vol. 2, pp. 1143–1186.
53 G. E. Ficken, in *The Chemistry of Synthetic Dyes*, ed. K. Venkataraman, Academic Press Inc., New York, 1971, vol. 4, pp. 211–334.
54 I. Horcas, R. Fernandez, J. M. Gomez-Rodriguez, J. Colchero, J. Gomez-Herrero and A. M. Baro, *Rev. Sci. Instrum.*, 2007, **78**, 13705–13713.
55 Peakfit is a product of Jandel Corporation, 2591 Rerner Boulevard, San Rafael, CA 94901, USA.
56 S. Monredon, C. Bonhomme, F. Ribot and F. Babonneau, *J. Sol-Gel Sci. Technol.*, 2009, **50**, 152–157.
57 R. J. Hook, *J. Non-Cryst. Solids*, 1996, **195**, 1–5.
58 S. Inagaki, S. Guan, T. Ohsuna and O. Terasaki, *Nature*, 2002, **416**, 304–307.
59 A. Shimojima, Y. Sugahara and K. Kuroda, *Bull. Chem. Soc. Jpn.*, 1997, **70**, 2847–2853.
60 Y. Fujimoto, A. Shimojima and K. Kuroda, *Chem. Mater.*, 2003, **15**, 4768–4774.
61 A. Shimojima and K. Kuroda, *Angew. Chem., Int. Ed.*, 2003, **42**, 4057–4060.
62 J. Clauss, K. Schmidt-Rohr, A. Adam, C. Boeffel and H. W. Spiess, *Macromolecules*, 1992, **25**, 5208–5214.
63 A. N. Parikh, M. A. Schivley, E. Koo, K. Seshadri, D. Aurentz, K. Mueller and D. L. Allara, *J. Am. Chem. Soc.*, 1997, **119**, 3135–3143.
64 L.-Q. Wang, J. Liu, G. J. Exarhos, K. Y. Flaniga and R. Bordia, *J. Phys. Chem. B*, 2000, **104**, 2810–2819.
65 L. D. Carlos, V. de Zea Bermudez, R. A. S. Ferreira, L. Marques and M. Assunção, *Chem. Mater.*, 1999, **11**(3), 581–588.
66 C. Bohm, F. Leveiller, D. Jacquemain, H. Mohwald, K. Kjaer, J. Als-Nielsen, I. Weissbuch and L. Leiserowitz, *Langmuir*, 1994, **10**, 830–836.
67 M. Fernandes, R. A. S. Ferreira X. Cattoën, L. D. Carlos, M. Wong Chi Man and V. de Zea Bermudez, *J. Sol-Gel Sci. Technol.*, DOI: 10.1007/s10971-012-2739-1.
68 S. S. Nobre, C. D. S. Brites, R. A. S. Ferreira, V. de Zea Bermudez, C. Carcel, J. J. E. Moreau, J. Rocha, M. Wong

Chi Man and L. D. Carlos, *J. Mater. Chem.*, 2008, **18**, 4172–4182.
69 S. C. Nunes, J. Planelles-Aragó, R. A. S. Ferreira, L. D. Carlos and V. de Zea Bermudez, *Eur. J. Inorg. Chem.*, 2010, **18**, 2688–2699.
70 J. F. Nagle and M. Goldstein, *Macromolecules*, 1985, **18**, 2643–2652.
71 M. D. Porter, T. B. Bright, D. L. Allara and C. E. D. Childsey, *J. Am. Chem. Soc.*, 1987, **109**, 3559–3568.
72 S. Singh, J. Wegmann, K. Albert and K. Muller, *J. Phys. Chem. B*, 2002, **106**, 878–883.
73 N. V. Venkataram and S. Vasudevan, *J. Phys. Chem. B*, 2001, **105**, 7639–7650.
74 N. V. Venkataram, S. Bhagyalakshmi, S. Vasudevan and R. Seshachi, *Phys. Chem. Chem. Phys.*, 2002, **4**, 4533–4538.
75 R. Wang, G. Baran and S. L. Wunder, *Langmuir*, 2000, **16**, 6298–6305.
76 R. A. Macphail, H. L. Strauss, R. G. Snyder and C. A. Ellinger, *J. Phys. Chem.*, 1984, **88**, 334–341.
77 R. G. Snyder, H. L. Strauss and C. A. Ellinger, *J. Phys. Chem.*, 1982, **86**, 5145–5150.
78 F. Bensebaa, Y. Zhou, A. G. Broto, D. E. Irish, Y. Deslandes, E. Kruss and T. H. Ellis, *Spectrochim. Acta, Part A*, 1999, **55**, 1229–1236.
79 K. G. Brown, E. Bicknell-Brown and M. Ladjadj, *J. Phys. Chem.*, 1987, **91**, 3436–3442.
80 D. J. Skrovanek, S. E. Howe, P. C. Painter and M. Coleman, *Macromolecules*, 1985, **18**, 1676–1683.
81 D. J. Skrovanek, P. C. Painter and M. M. Coleman, *Macromolecules*, 1986, **19**, 699–705.
82 N. B. Colthup, L. H. Daly and S. E. Wiberley, *Introduction to Infrared and Raman Spectroscopy*, Academic Press, San Diego, CA, 1990.
83 R. A. S. Ferreira, A. L. Ferreira and L. D. Carlos, *Eur. Phys. J. B*, 2006, **50**, 371–378.